Heliyon 10 (2024) e39752

Contents lists available at ScienceDirect

Heliyon

journal homepage: www.cell.com/heliyon

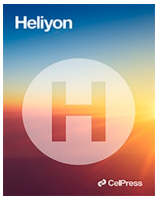

Research article

TPC1 regulates melanoma tumourigenesis via mTORC1 and TFEB

Xuhui Jin [a,1], Ali A. Hanbashi [a,b], Faroq Kamli [a,b], Xiaoqi Pan [c], Colin R. Goding [d], John Parrington [a,*]

[a] Department of Pharmacology, University of Oxford, Mansfield Road, Oxford, OX1 3QT, United Kingdom
[b] Department of Pharmacology, College of Pharmacy, Jazan University, Jazan, 45142, Saudi Arabia
[c] State Key Laboratory of Southwestern Chinese Medicine Resource, Chengdu University of Traditional Chinese Medicine, 611137, Chengdu, China
[d] Ludwig Institute for Cancer Research, Nuffield Department of Clinical Medicine, Old Road Campus, University of Oxford, Oxford, OX3 7DQ, United Kingdom

ARTICLE INFO

Keywords:
TPC1
TFEB
mTORC1
MITF
Melanoma

ABSTRACT

The major cause of death in cancer patients is a combination of metastatic dissemination combined with therapy resistance. Over recent years, intratumour phenotypic heterogeneity arising from the bi-directional interplay between plastic cancer cells and the microenvironment has been identified as key to disease progression. Most notably metastatic outgrowth and resistance to targeted therapies are frequently associated with activity of mTORC1, a key metabolic hub that promotes protein synthesis and proliferation in the presence of nutrients. Yet while the regulation of mTORC1 by amino acids and glucose availability is well characterized, whether other mechanisms are important in controlling mTORC1 and its downstream signalling is less well understood. Here we show, using the murine B16-F0 melanoma cell line as a model, that mTORC1 activity is decreased following the knockout (KO) of TPC1, a cation channel localised to early and recycling endosomes. Consequently, TPC1 KO melanoma cells exhibit reduced proliferation and invasiveness, as well as increased pigmentation associated with nuclear localisation of the MITF-related transcription factor TFEB. Our results demonstrate that the knockout of TPC1 has induced significant tumour-suppressive effects in melanoma, during which the altered activity of mTORC1 and TFEB play the key roles. The results help us further understand the link between mTORC1 and endolysosomal ion channels, and reveal that TPC1 controls melanoma progression and represents a potential therapeutic target.

1. Introduction

Beyond the initial genetic events that promote cancer initiation, it is increasingly recognised that tumour growth is accompanied by the generation of multiple different phenotypic states that can coexist. Each phenotype will share the same genetic driver mutations, but may exhibit profoundly different biological properties ranging from differentiation to proliferation, invasion, and dormancy [1]. Moreover, while therapy resistance in many cancers has been linked to genetic mutations, it is now also clear that some phenotypic states exhibit tolerance to treatments including targeted therapies and immunotherapies [2]. The generation of different phenotypes occurs because epigenetically plastic cancer cells adopt survival strategies in response to stresses encountered within their local

* Corresponding author.
E-mail address: john.parrington@worc.ox.ac.uk (J. Parrington).
[1] Present Address: Basic Sciences Division, Fred Hutchinson Cancer Center, Seattle, WA, 98109, United States.

https://doi.org/10.1016/j.heliyon.2024.e39752
Received 21 May 2024; Received in revised form 9 September 2024; Accepted 22 October 2024
Available online 23 October 2024

microenvironment, such as hypoxia, nutrient limitation, and inflammatory signalling [3]. Understanding how cells tailor their responses to stress and how this impacts invasion, metastatic dissemination and outgrowth is therefore a key issue.

Melanoma represents an excellent model to understand how the drivers and effectors of phenotype switching affect disease progression. In part, this is because of the identification of the microphthalmia-associated transcription factor (MITF), a key regulator of many aspects of melanoma biology, including metabolism, whose expression and activity marks different phenotypic states; low MITF is associated with invasion, but high MITF is tied to either proliferation, or differentiation characterized by production of the pigment melanin and melanosomes. As such, microenvironmental stresses that promote invasion also lead to down-regulation of MITF, both transcriptionally and through suppression of its translation via phosphorylation of the translation initiation factor eIF2α downstream from the integrated stress response [4,5].

In addition to controlling genes linked to differentiation and proliferation, MITF has also been implicated in regulation of endolysosomal and lysosomal biogenesis, the v-ATPase complex, and autophagy, raising the possibility of feedback from endosomes and lysosomes to MITF expression [6]. One way this might be achieved is via the activity of the mammalian target of rapamycin complex 1 (mTORC1) that senses amino acids at the lysosome surface, to promote protein synthesis and suppress autophagy. mTORC1 activity is frequently associated with resistance to targeted therapies and phosphorylates the MITF-related factor, transcription factor EB (TFEB), that is then retained in the cytoplasm [7]. Although the role of TFEB in melanoma is poorly understood, its expression can suppress that of MITF, providing a mechanistic link whereby inhibition of mTORC1 can reduce MITF expression [8]. However, whether other lysosome or endosome-associated proteins can also regulate MITF or its related factors is not known.

Two-pore channels (TPC) are a group of cation channels located on the surface of the endolysosomal system that are permeable primarily to Ca^{2+}, Na^{+} and H^{+}, and contribute to intracellular Ca^{2+} signalling [9,10]. In humans and most rodents, there are two isoforms, TPC1 and TPC2 (encoded by the *TPCN1* and *TPCN2* genes in human, and *Tpcn1* and *Tpcn2* genes in mice) [11]. TPC1 is more prevalent in early and late endosomes, while TPC2 is predominantly found in lysosomes [12]. Significantly, TPCs have been implicated in a wide range of diseases, including melanoma and other types of cancer [13], and recent gene expression analysis showed that the levels of TPC2 mRNA transcripts were upregulated in two melanoma cell lines [5]. In addition, TPC2 is important in melanoma progression since a TPC2 knock-out in CHL-1 melanoma cells promoted invasiveness and increased metastatic potential [14]. In contrast, a different study showed the opposite, namely that TPC2 knockout (KO) in MNT-1 cells reduced their aggressiveness [15]. A notable difference between these two cell lines is that CHL-1 is $MITF^{Low}$ and has lost its melanin-producing ability, while MNT-1 is $MITF^{High}$ and retains its melanotic potential [16]. In the MNT-1 study, melanogenesis was elevated by TPC2 KO [15] suggesting that it could regulate MITF activity. However, the potential role of TPC1 in melanoma remains unknown.

Here, for the first time, we explore the role of TPC1 in melanoma progression, using wild-type (WT) and TPC1 KO melanoma cells to investigate the effect of TPC1 loss of function on molecular and cellular parameters associated with melanoma tumourigenesis and metastasis.

2. Materials and methods

2.1. Cell culture

B16-F0 cells (WT, TPC2 KO) were obtained from a previous study [14]. Cells were cultured in DMEM medium (with L-glutamine) (Gibco, 11995-065), which was supplemented with 10 % foetal bovine serum (FBS) and antibiotics (100 U/mL penicillin, 100 μg/mL streptomycin). Cells were maintained at 37 °C with 5 % CO_2 and humidity. Absence of mycoplasma contamination was checked by PCR on a monthly basis (primer sequence: forward GGGAGCAAACAGGATTAGATACCCT, reverse TGCACCATCTGTCACTCTGTTAACCTC).

2.2. CRISPR/Cas9

The sgRNAs for CRISPR/Cas9 gene editing were designed using the Synthego CRISPR Design Tool (https://design.synthego.com) to minimise off-target effects. sgRNA (sequence: CCACAGCAUCCACAACUCCC) and *S. pyogenes* Cas9 nuclease (Synthego) were mixed and transfected into cells in suspension using CRISPRMAX™ Reagent (Invitrogen™, CMAX00003). The number of cells and the ratio between sgRNA and Cas9 (which ranged from 1:1 to 9:1) were optimised to maximise efficiency. Following transfection, DNA was extracted from the cells using a Wizard® Genomic DNA Purification Kit (Promega, A1120), and the edited region of *Tpcn1* gene was amplified by PCR (primer sequence: forward GCACATGGACAGACTGACCA, reverse CCGGGCACACAAGTTCCTAT). The PCR products were purified with ExoSAP-IT™ Reagent (Applied Biosystems™, 78201), and then sequenced with a 3730xl DNA Analyzer (Applied Biosystems™). The sequencing data was analysed using an ICE CRISPR Analysis Tool (Synthego, https://ice.synthego.com) for indel and KO scores. Cells with high KO scores were sorted into single cells using FACSAria™ III Cell Sorter (BD Biosciences) for clonal expansion.

2.3. RT-qPCR

RNA purification was performed using a GeneJET RNA Purification Kit (Thermo Scientific™, K0731), and the extracted RNA was converted to cDNA with a High-Capacity RNA-to-cDNA™ Kit (Applied Biosystems™, 4387406). For qPCR, the cDNA template was mixed with primers and PowerUp™ SYBR™ Green Master Mix (Applied Biosystems™, A25742), and was run with LightCycler® 480 System (Roche®). A thermocycle consisted of UDG activation at 50 °C for 2 min, DNA polymerase activation at 95 °C for 2 min, and 40

cycles of DNA amplification (DNA denaturation at 95 °C for 15 s and annealing/extension at 60 °C for 1 min). GAPDH and β-actin were used as internal controls, and their geometric means were used to quantify cDNA of interest following the $2^{-\Delta\Delta Ct}$ methAod [17]. The primer sequences were as below:

Primers:
TPC1 F: 5′-TCCAAGGCCTTCCAGTATTTC -3′
R: 5′-CTCCACCAGGATCCAGACAC-3’
TPC2 F: 5′-GAGCTCTGCATAGACCAGGCTGTGG-3′
R: 5′-CCAGGAAGGCAAGCAAGCAGAACGC-3’
Total MITF F: 5′-CGTGTATTTTTCCCACAGAGTC-3’
R: 5′-GCTCCTTAATGCGGTCGTTTA-3’
MITF-A F: 5′-GCGGATTTCGAAGTCGGGGAGG-3′
MITF-B F: 5′-GAGTGCCATGCCGTGCCTTGAT-3′
MITF-C F: 5′-TTTTCCCACCAGCTGATTCCTCTA-3′
MITF-D F: 5′-GTTGGGACCTGACAGGCTCTGAATACAG-3′
MITF-E F: 5′-GGAAGATTAAGCCCAGTGAGGTT-3′
MITF-H F: 5′-GGGCTTGCAGAACACCTTAAAGG-3′
MITF-J F: 5′-TCTCGCCGTGTCTCTGGGCATC-3′
MITF-Mc F: 5′-ACACAAGCCCTACCTCAGAACC-3′
Universal MITF Reverse (except MITF-M)
R: 5′-GCACGCTGACGTTTATGGCTGG-3′
MITF-M F: 5′-TATGGTGCCTTCTTTATGCC-3′
R: 5′-AGCATAGCAAGGTTTCAGG-3′
Tyr F: 5′-CAAAGGGGTGGATGACCGTG-3′
R: 5′-AACTTACAGTTTCCGCAGTTGA-3′
Tyrp1 F: 5′-CCCCTAGCCTATATCTCCCTTTT-3′
R: 5′-TACCATCGTGGGGATAATGGC-3′
Dct F: 5′-TTCCCCGAGTCTGCATGAC-3′
R: 5′-TGCATGTCCGGTTGAAGAATTT-3′
Raptor F: 5′-CTGCCCTTGCCAGATGAGAA-3′
R: 5′-CAGGCCTGGAGGGGTAGATA-3′
β-actin F: 5′-GTGACGTTGACATCCGTAAAGA-3′
R: 5′-GCCGGACTCATCGTACTCC-3′
GAPDH F: 5′-GGAGCGAGATCCCTCCAAAAT-3′
R: 5′-GGCTGTTGTCATACTTCTCATGG-3′

2.4. Western blot

For protein extraction, the cells were lysed in RIPA lysis buffer (Thermo Scientific™, 89900), supplemented with a protease and phosphatase inhibitors cocktail, and then centrifuged at 14,000 g for 15 min at 4 °C. The supernatant containing dissolved protein was kept, and the concentration was quantified using a bicinchoninic acid (BCA) assay (Sigma-Aldrich, B9643). For the Western blot, 25 μg denatured protein was separated by TGX™ Protein Gel (Bio-Rad, 4561094) and transferred to a PVDF membrane. The membrane was incubated with the following primary antibodies at 4 °C overnight: anti-TPC1 (1:1000, LSBio, LS-C110014), anti-MITF (1:1000, Abcam, ab12039), anti-Raptor (1:1000, Cell Signaling Technology, 2280), anti-S6K (1:1000, Abcam, ab32529), anti-pS6K (1:1000, Cell Signaling Technology, 9204), and anti-TFEB (1:1000, Cell Signaling Technology, 83010). Anti-β-actin (1:1000, Cell Signaling Technology, 3700) and anti-GAPDH (1:1000, Cell Signaling Technology, 97166) were incubated with the membrane at room temperature for 1 h as loading controls. Secondary antibodies against relevant species were used as follows: anti-rabbit (1:2500, Abcam, ab216773) and anti-mouse (1:2500, Abcam, ab216778). The membrane was imaged by Odyssey® M Imaging System (LI-COR) and the blots were analysed by Fiji/ImageJ (version 1.54c) [18].

2.5. Immunocytochemistry

Cells were seeded onto sterilised coverslips which were pre-coated with poly-D-lysine. When the cells reached 70 %–80 % confluency, the coverslips were removed and washed. The cells were then fixed with paraformaldehyde (4 % in PBS) for 10 min and permeabilised with Triton X-100 (0.1 % in PBS) for another 10 min. Bovine serum albumin (BSA) (1 % in PBST) was used to block the coverslip for 1 h. Then the coverslips were incubated with anti-MITF (1:100, Cell Signaling Technology, 97800) or anti-TFEB (1:100, Cell Signaling Technology, 83010) primary antibodies at 4 °C overnight in a humidified chamber. On the second day, Alexa Fluor™ 546-conjugated anti-rabbit (1:1000, Invitrogen™, A11071) secondary antibodies were used to incubate the coverslips at room temperature for 1 h. After extensive washing, the coverslips were mounted on microscope slides with ProLong Gold Antifade Reagent (with DAPI) (Invitrogen™, P36935). The image was captured by Zeiss LSM 710 Confocal Microscope and quantified with Fiji/ImageJ (version 1.54c) by measuring the fluorescence intensity after being normalised to background [18].

2.6. Cell proliferation assay

Cell viability was determined using both a direct cell counting assay and an MTT assay [19]. For cell counting, cells were trypsinised and stained with Trypan blue, and were counted using a Countess™ Automated Cell Counter (Invitrogen™). For the MTT assay, cells were seeded into 96-well plates at a density of 2,000 cells/well. Upon measurement, the cells were incubated with 10 % MTT salt for 4 h. Then DMSO was used to dissolve the yielded formazan salt. The colourimetric absorbance was measured at 595 nm using a Sunrise™ Microplate Reader (TECAN). Day 0 viability was also measured to calibrate the error due to initial seeding numbers.

2.7. Melanin and tyrosinase activity

For extracellular melanin release, cells were seeded into 24-well plates with 50,000 cells/well in colourless DMEM medium (Gibco, 31053-028). Upon measurement, the medium was transferred into 96-well plates for absorbance measurement at 405 nm using a Sunrise™ Microplate Reader (TECAN). Day 0 viability was measured using an MTT assay to calibrate the error due to initial seeding numbers.

For intracellular melanin content, the protein was extracted and quantified as described above. Then the centrifugation pellet was

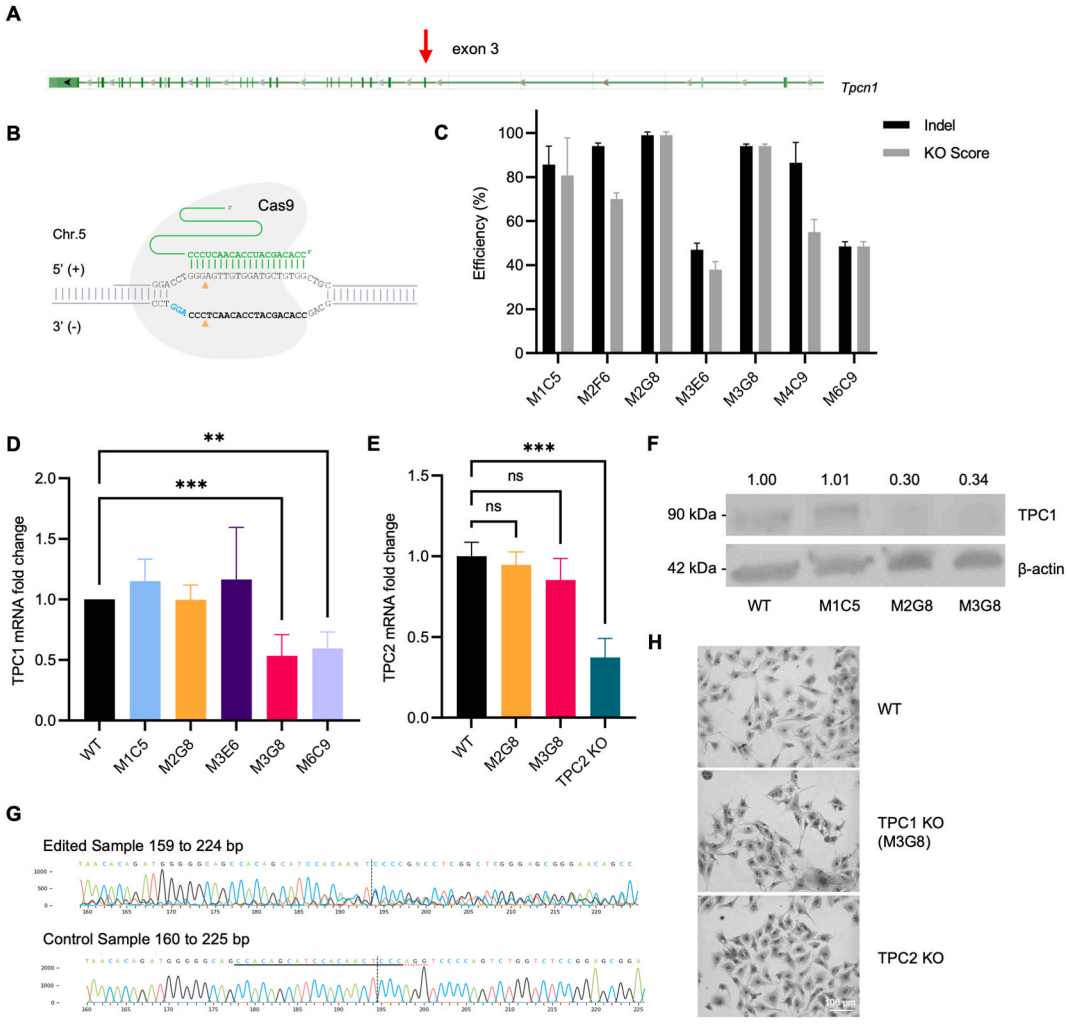

Fig. 1. The generation of TPC1 KO B16-F0 cell models. (A) The location of exon 3 in the murine *Tpcn1* transcript. (B) A schematic illustration of the CRISPR design and the sequence of the sgRNA. (C) Analysis of editing efficiency of possible TPC1 KO cell colonies (n = 3). Indel indicates the percentage of edited DNA, and KO scores indicate effective KO (i.e. frameshift or large insertion/deletion). Colonies M2G8 and M3G8 showed consistently high KO scores. (D–E) Levels of *Tpcn1* and *Tpcn2* mRNA expression in potential TPC1 KO cell lines as assessed by RT-qPCR (n = 3). Colony M3G8 showed a significant drop of the level of *Tpcn1* transcription compared to WT cells while the level of *Tpcn2* transcription was not affected. **p < 0.01, ***p < 0.001, one-way ANOVA with Dunnett's test. (F) TPC1 protein was not detected in the M3G8 colony. (G) Given all the results above, colony M3G8 was chosen for further study. Sanger sequencing showed that the codon sequence had been altered by CRISPR. (H) Compared with WT or TPC2 KO B16-F0 cells, TPC1 KO cells have similar morphological properties.

collected, and heated in 1M NaOH (in 10 % DMSO) at 80 °C for 2 h. After cooling down to room temperature, the absorbance of the solution was measured at 405 nm using a Sunrise™ Microplate Reader (TECAN). The absorbance was compared to a calibration curve to determine protein concentration.

For tyrosinase activity, 100 μg of extracted protein was taken and diluted in 100 μL PBS. 50 μL of 15 mM L-dopa was added to the diluted protein, and the mixture was incubated at 37 °C for 30 min to obtain a colour change. After cooling down to room temperature, the absorbance of the solution was measured at 495 nm on a Sunrise™ Microplate Reader (TECAN).

2.8. Cell migration and invasiveness

For the wound healing assay, cells were seeded into 6-well plates at a density of 3×10^5 cells/well. Mitomycin (10 μg/mL) was added to inhibit cell proliferation. After the cells formed a confluent monolayer, 200 μL pipette tips were used to make a straight scratch (the "wound") in the middle of the wells. Images of cells were captured using an EVOS™ FL Auto 2 Imaging System (Invitrogen™) to record the area of the wound at different time points. The area of the wound was quantified by Fiji/ImageJ (version 1.54c) [18].

For the transwell migration assay, 5×10^5 cells were loaded into a transwell insert (8 μm pore size) (Sarstedt, 83.3930.800) with 2

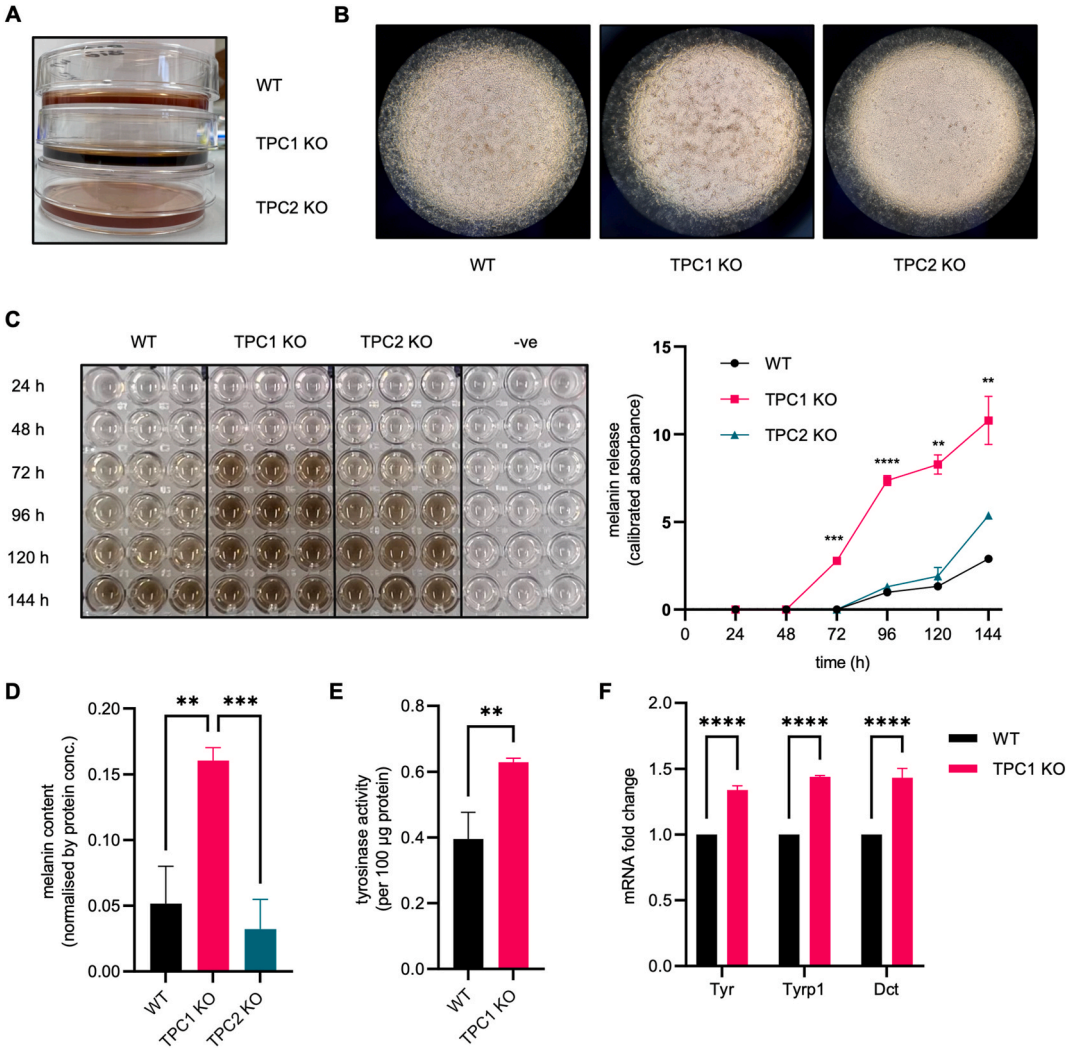

Fig. 2. TPC1 KO increased the production of melanin in B16-F0 cells. (A) The colour of DMEM medium when the cells reached confluency. From top to bottom: WT, TPC1 KO, TPC2 KO. (B) A microscopic view of confluent cell culture. TPC1 KO cells had more melanin aggregates. (C) The measurement of extracellular release in colourless DMEM medium (n = 3). After 72 h, TPC1 KO cells began to show substantially increased melanin release. **p < 0.01, ***p < 0.001, ****p < 0.0001, two-way ANOVA with Tukey's test. (D) The level of intracellular melanin content (n = 3). TPC1 KO cells had more melanin within the cells. **p < 0.01, ***p < 0.001, one-way ANOVA with Dunnett's test. (E) Increased level of tyrosinase activity in TPC1 KO cells (n = 3). **p < 0.01, *t*-test. (F) Increased levels of *Tyr*, *Tyrp1*, and *Dct* mRNAs in TPC1 KO cells (n = 3). ****p < 0.0001, *t*-test.

μL serum-free DMEM medium. The inserts were then placed in 6-well plates with 2 μL complete DMEM medium per well as a chemoattractant. After incubation at 37 °C for 24 h, all medium was removed, and the transwell inserts were carefully washed twice in PBS. Then paraformaldehyde (4 % in PBS) was applied to fix the cells at room temperature for 2 min. Gram's crystal violet solution (1:200 diluted in 20 % methanol) was used to stain the cells at room temperature for 10 min. After proper washing, non-migrated cells at the top surface of the transwell inserts were gently scraped off by cotton swabs. The images of migrated cells were captured using an EVOS™ FL Auto 2 Imaging System (Invitrogen™). For quantification, 33 % acetic acid was used to elute Gram's crystal violet on a shaker for 10 min, and the eluants were collected for absorbance reading at 595 nm using a Sunrise™ Microplate Reader (TECAN).

For the transwell invasion assay, the same steps were followed, except that the top surface of transwell inserts were pre-coated with 500 μL ECM gel (0.5 mg/mL in serum-free DMEM medium) (Sigma-Aldrich, E1270).

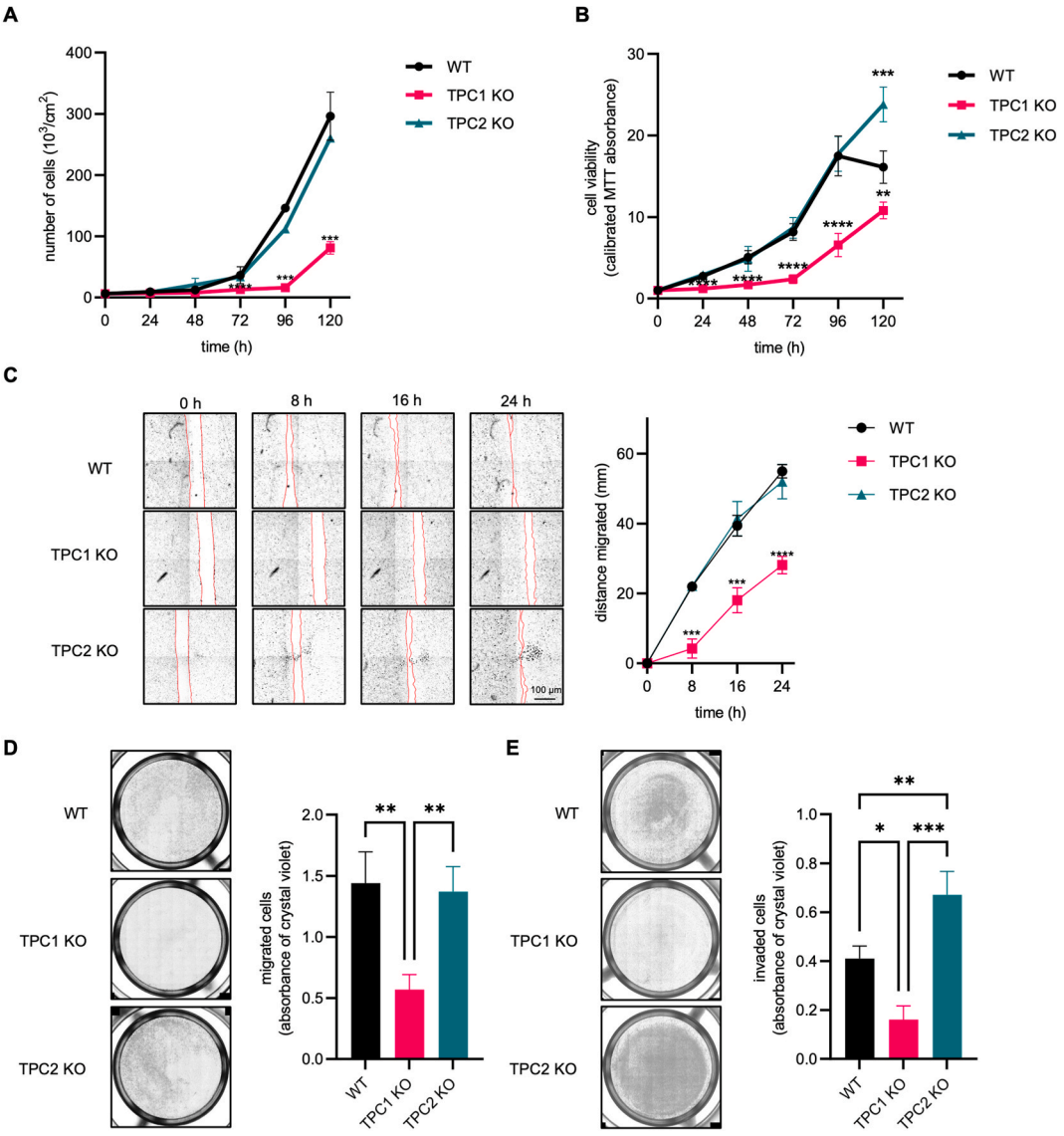

Fig. 3. TPC1 KO reduced the rate of proliferation, migration and invasiveness of B16-F0 cells. (A–B) Rate of proliferation as assessed by a cell counting assay and an MTT assay (n = 6). TPC1 KO cells showed significantly reduced proliferation rates. **p < 0.01, ***p < 0.001, ****p < 0.0001, two-way ANOVA with Tukey's test. (C) Rate of cell migration as assessed by wound healing assay (n = 4). TPC1 KO cells recovered the wound at a slower rate. ***p < 0.001, ****p < 0.0001, two-way ANOVA with Tukey's test. (D) Rate of cell migration within 24 h as assessed by transwell assay (n = 3). Less TPC1 KO cells were able to migrate across the transwell after 24 h, compared with WT and TPC2 KO cells. **p < 0.01, one-way ANOVA with Dunnett's test. (E) An assessment of cell invasiveness within 24 h (n = 3). ECM gel was coated onto transwells, and TPC1 KO cells showed reduced ability of breaking ECM while TPC2 KO cells exhibited the opposite characteristic. *p < 0.1, **p < 0.01, ***p < 0.001, one-way ANOVA with Dunnett's test.

2.9. Statistics

All data were presented as mean with SD. Depending on the nature of the data, student's t-test, one-way ANOVA or two-way ANOVA (with post-hoc Tukey tests) were used as appropriate. P values were reported as ns ($P > 0.05$), * ($P \leq 0.05$), ** ($P \leq 0.01$), *** ($P \leq 0.001$) and **** ($P \leq 0.0001$). GraphPad Prism (version 9.2.0, GraphPad Software) was used to analyse and present the data.

3. Results

3.1. Expression of TPC1 abolished in B16-F0 cells

In order to generate a TPC1-deficient cell model, we exploited CRISPR/Cas9 gene editing to knock out the *Tpcn1* gene in mouse

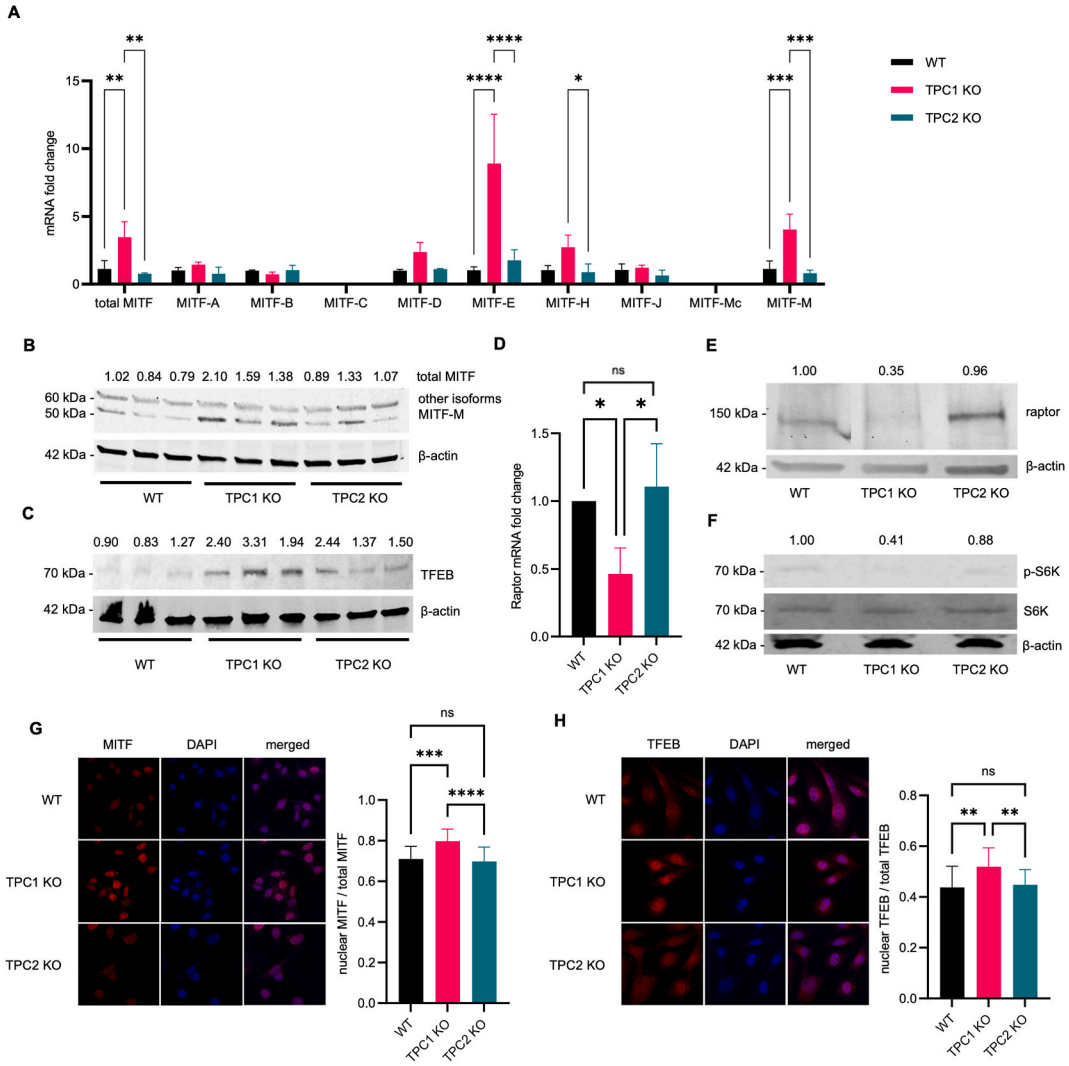

Fig. 4. MITF and TFEB are hyperactive in TPC1 KO B16-F0 cells, as a result of downregulated mTORC1 complex activity. (A) The mRNA levels of MITF and its isoforms (n = 3). In TPC1 KO cells, the mRNA transcript levels of total MITF and isoforms E, H and M were upregulated. *p < 0.1, **p < 0.01, ***p < 0.001, ****p < 0.0001, one-way ANOVA with Dunnett's test. (B) The protein level of MITF (n = 3). MITF-M has a smaller molecular weight than other isoforms, which makes it differentiable by Western blot. TPC1 KO cells had more MITF-M protein expressed. (C) The protein level of TFEB (n = 3). TFEB was overexpressed in TPC1 KO cells. (D–E) The protein and mRNA level of Raptor, a mTORC1-specific subunit (n = 3). Raptor was downregulated in TPC1 KO cells. *p < 0.1, one-way ANOVA with Dunnett's test. (F) The level of total and phosphorylated S6 kinase. The intracellular phosphorylation of S6 kinase is exclusively achieved by mTORC1. Here TPC1 KO cells showed reduced phospho-S6 kinase signal, indicating mTORC1 was hypoactive. (G) Intracellular localisation of MITF (n > 20). MITF were more localised to the nucleus in TPC1 KO cells. ***p < 0.001, ****p < 0.0001, one-way ANOVA with Dunnett's test. (H) Intracellular localisation of TFEB (n > 20). TFEB were more localised to the nucleus in TPC1 KO cells, and showed an increased fluorescence intensity in TPC1 KO cells. **p < 0.01, one-way ANOVA with Dunnett's test.

B16-F0 melanoma cells. A single guide RNA (sgRNA) was designed to target exon 3 to ensure that a CRISPR-induced codon frameshift could sufficiently disrupt all downstream translation (Fig. 1A and B). This meant that the truncated isoform, *Tpcn1B*, which lacks complete exons 1 and 2 [20], would also be knocked out. Following CRISPR/Cas transfection, single cell sorting and clonal expansion, a few single cells developed into colonies and showed reasonable levels of indel (insertion or deletion of bases) or KO scores (an indel that results in a frameshift or has more than 30 bases inserted/deleted) (Fig. 1C). Among these colonies, M3G8 showed consistently high indel and KO scores. Further investigation also showed that in this colony the level of *Tpcn1* mRNA decreased by 50 % and the encoded TPC1 protein was undetectable by Western blot (Fig. 1D and F). To examine the specificity of gene editing and potential compensatory expression by TPC2, we checked the level of *Tpcn2* mRNA in the M3G8 colony, and confirmed that TPC1 KO did not affect the expression of TPC2 (Fig. 1E). Given the evidence, we chose colony M3G8 for future study. Morphologically, these TPC1 KO cells did not exhibit any significant differences from WT or TPC2 KO cells (Fig. 1H).

3.2. TPC1 KO increases melanogenesis

Following the generation of TPC1 KO B16-F0 cells, one of the most notable phenotypic changes in the KO cells was that both the culture medium (Fig. 2A) and the cells (Fig. 2B) showed increased pigment accumulation. The level of extracellular melanin was measured by seeding cells in a 96 well plate in colourless medium to eliminate any interference from phenol red, and the medium colour change determined by measuring absorbance over time at 405 nm. Initially, there was no significant difference due to the relatively low cell numbers. After 48 h, however, TPC1 KO cells began to show drastically more melanin release into the medium, and this trend continued for the rest of the experiment (Fig. 2C). To further investigate the source of the increased melanin release, we next measured the level of intracellular melanin. We found that TPC1 KO cells also showed significantly higher intracellular melanin levels, which were around three times that in WT and TPC2 KO cells (Fig. 2D). These findings indicate that the increased melanin release was most likely due to increased melanin synthesis. To verify this, we measured the activity of tyrosinase (Tyr) in the protein extracts. As the principal enzyme for melanin synthesis, tyrosinase converts L-tyrosine to an intermediate product, L-dopa, and then to different types of melanin [21]. We added L-dopa to cell protein extracts and measured the colour change. This analysis showed that the tyrosinase activity was higher in TPC1 KO cells than in WT or TPC2 KO cells (Fig. 2E). Furthermore, RT-qPCR analysis showed that the level of *Tyr* mRNA transcripts was also upregulated, as were the mRNAs encoding the accessory proteins that are required for Tyr activity, Tyrp1 and Dct (Fig. 2F). Collectively these findings show that loss of TPC1 leads to increased melanogenesis in B16-F0 cells.

3.3. TPC1 KO cells show decreased proliferation, migration and invasiveness

Since previous studies have suggested that TPC2 KO has an impact on melanoma aggressiveness [14,15], we also examined the influence of TPC1 KO on tumourigenic and metastatic parameters. First, we assessed the rate of proliferation using both a cell counting assay and an MTT assay [19]. Compared with WT and TPC2 KO cells, TPC1 KO cells showed a much lower rate of proliferation, especially at early times. (Fig. 3A and B). Next we measured the migratory and invasive ability of the cells by a scratch wound-healing assay and a transwell assay respectively. In both assays TPC1 KO cells showed attenuated migration/invasion: in the wound healing assay it took longer for TPC1 KO cells to repair the wound (Fig. 3C), and in the transwell assay fewer TPC1 KO cells were able to migrate through the pores compared with WT and TPC2 KO cells (Fig. 3D). The increased potential for invasion associated with cells lacking TPC1 was reflected in their decreased ability to invade by breaking down a layer of extracellular matrix (ECM) gel applied to the transwell (Fig. 3E). In this assay, we observed that TPC2 KO cells also showed increased invasiveness. Our findings suggest that TPC1 KO B16-F0 cells might have reduced metastatic potential. In summary, the loss of TPC1 in B16-F0 cells was associated with a tumour-suppressor effect, with TPC1 KO significantly delaying cell growth, migration, and invasiveness.

3.4. Upregulation of TFEB is associated with TPC1 KO

To further investigate the underlying molecular mechanisms of the phenotypic changes in TPC1 KO B16-F0 cells, we first measured the level of MITF, a key coordinator of melanocyte and melanoma cell growth, migration, invasion, melanin production, and cell survival [4]. To date, more than 10 different isoforms of MITF have been identified, among which the melanocyte-specific MITF-M protein plays particularly key roles in regulating cellular events [22]. By performing RT-qPCR using isoform-specific primers we detected overexpression of total MITF, MITF-E, MITF-H, and importantly, MITF-M, in TPC1 KO cells compared to WT (Fig. 4A). By contrast expression in TPC2 KO cells was similar to that in WT cells. MITF-C and MITF-Mc are specific to other cell types and were not detected [23,24]. Uniquely, MITF-M has a reduced molecular weight, which has made it differentiable by Western blot [25], owing to a smaller exon 1 compared with other isoforms. We took advantage of this property and detected a minor increase in expression of MITF-M at the protein level in TPC1 KO cells (Fig. 4B). MITF is a member of a family of closely related transcription factors that includes TFEB, a known regulator of MITF expression [8]. We therefore also asked whether TFEB expression was affected in TPC1 KO cells. Compared to WT cells, western blotting revealed up-regulation of TFEB protein levels in TPC1 KO cells, but not in cells lacking TPC2 (Fig. 4C). Both TFEB and non-MITF-M MITF isoforms are regulated by the mammalian target of rapamycin complex 1 (mTORC1), a key metabolic hub that is activated at the surface of the lysosome in the presence of amino acids. In nutrient rich conditions, mTORC1 phosphorylates TFEB and non-MITF-M MITF isoforms which prevents them from entering the nucleus [7]. To investigate whether changes in mTORC1 activity might be the cause of MITF and/or TFEB hyperactivity in TPC1 KO cells, we examined the level of Raptor, an mTORC1-specific subunit protein [26]. We found that Raptor was downregulated in TPC1 KO cells, but not in cells lacking TPC2, at both the mRNA and protein level (Fig. 4D and E). We therefore examined by western blotting the phosphorylation status of S6 kinase, a

key mTORC1 target commonly used as an indicator of mTORC1 activity [27]. Compared to WT or TPC2 KO cells, we observed a decrease of phosphorylated S6 kinase in TPC1 KO cells (Fig. 4F). Collectively, these data imply that the activity of mTORC1 is suppressed in TPC1 KO cells. To verify that changes in mTORC1 activity are correlated with changes in the intracellular localisation of MITF and TFEB, we further performed immunofluorescence on these two proteins, and found that in TPC1 KO cells both showed higher levels of nuclear localisation than in WT or TPC2 KO cells (Fig. 4G and H). This further suggests that TFEB and MITF are more active as transcription factors in cells lacking TPC1.

4. Discussion

A feature of MITF is that its functions are correlated with its level of expression, which is known as the "rheostat model": in the low state, it triggers cell senescence; in the intermediate state, it upregulates the expression of genes that control cell proliferation, migration, and invasiveness; and in the high state, melanoma cells tend to produce more melanin and show increased differentiative traits [5,28]. Our findings in this study show that TPC1 KO B16-F0 cells have increased levels of MITF and melanin, and reduced proliferation, migration, and invasiveness, indicating that knockout of TPC1 switches MITF from an intermediate to a high state. We also demonstrated the downregulation of mTORC1 activity in TPC1 KO cells which would lead to increased nuclear accumulation of TFEB, an MITF-related factor that binds and regulates similar genes to MITF.

Interestingly, as the key isoform in melanocytes, MITF-M is not regulated by mTORC1 due to it lacking an N-terminal motif responsible for lysosomal targeting that is conserved in other isoforms [8]. Nonetheless, a recent finding indicated that MITF-M expression is closely mediated by TFEB [8], and thus mTORC1 might still exert influence on MITF-M via an indirect mechanism involving TFEB. The functions of TFEB are closely related to lysosome biology, including lysosomal biogenesis, homeostasis, and autophagy [29]. The roles of TFEB have been described in various types of cancer [30]. In melanoma, it was shown that TFEB could be upregulated by inhibiting mutated $BRAF^{V600E}$, which, in line with our observations in TPC1 KO cells, led to a tumour-suppressor effect [31]. Considering the high prevalence of the $BRAF^{V600E}$ mutation (around 50 % in all melanoma cases) [32], our work provides new insights into the molecular mechanisms of $BRAF^{V600E}$-induced oncogenesis, as well as providing a novel approach for targeted melanoma treatment.

As a lysosome-bound protein complex, mTORC1 is mainly involved in energy metabolism, nutrient processing, and redox homeostasis [33]. Previous work has indicated that mTORC1 could have a crosstalk with TPCs. However, the detailed mechanism is still unclear as existing pieces of evidence are controversial. In some studies, mTORC1 was able to participate in TPC activation [34,35], while ATP-dependent mTORC1-induced TPC inhibition has also been observed [36]. Another study showed that TPC2 could in turn trigger mTORC1 activation [37]. Therefore one could draw the conclusion that mTORC1 indeed has crosstalk with TPC, but how

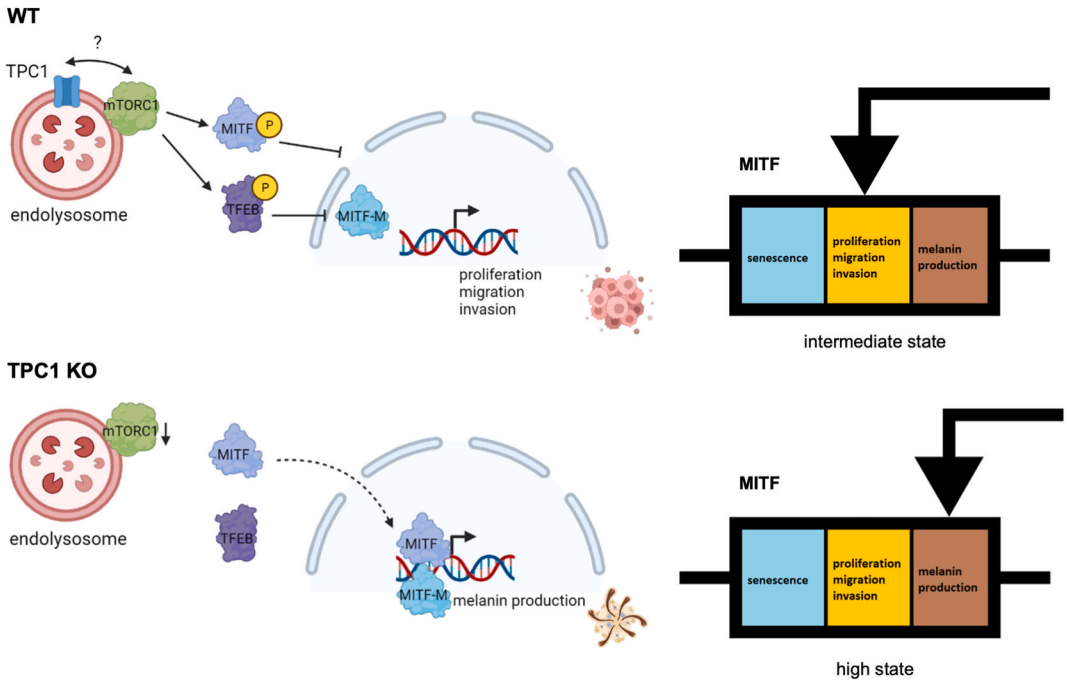

Fig. 5. A hypothesised pathway of the tumour suppressor effect of TPC1 KO in B16-F0 cells. The loss of TPC1 attenuates the activity of the mTORC1 complex, which mitigates the phosphorylation-induced inhibition on TFEB. On the one hand, this further elevates the level of MITF-M in the nucleus. On the other hand, other MITF isoforms whose activity is directly inhibited by mTORC1 are also released from this inhibition. Collectively these effects boost the nuclear activity of MITF, which switches the MITF "rheostat" from "intermediate" to "high" state. Thus the TPC1 KO cells appear to produce more melanin while showing decreased proliferative, migrative and invasive abilities. The image was created with BioRender.

exactly it works has remained unclear. Here based on our findings we hypothesise that the loss of TPC1 in B16-F0 cells has attenuated the activity of mTORC1 and subsequently hyperactivated MITF due to reduced phosphorylation. It was already shown that hyperactivated MITF could in turn stabilise MITF *per se* through the Wnt signalling pathway, forming a positive feedback loop [38]. Eventually the increased MITF and TFEB stimulate a series of cell events that lead to a tumour-suppressive state (Fig. 5). In summary, we suggest that TPC1 could regulate melanoma progression via the mTORC1-TFEB-MITF axis, which may provide a novel connection between cancer progression, autophagy, melanin production, energy metabolism, and Ca^{2+} homeostasis.

Another interesting finding in this study was the behaviour of TPC2 KO cells. In most of our assays TPC2 KO cells showed similar traits to WT cells, except that they exhibited increased invasiveness, which is in line with the discovery made previously by us about the effect of TPC2 KO in CHL-1 cells [14]. Nonetheless, there are notable differences between our findings here about the effect of TPC2 KO in B16-F0 cells, and our previous findings, namely that the TPC2 KO CHL-1 cells also had increased adhesive properties and overexpression of MITF [14]. On the other hand, the findings of another previous study into the effects of TPC2 KO in MNT-1 cells, which showed increased MITF and melanin, and decreased invasiveness [15], are very similar to our findings here regarding the effects of TPC1 KO in B16-F0 cells, although we did not see such significant changes in our TPC2 KO B16-F0 cells. A major difference between B16-F0 and MNT-1 cell lines is that B16-F0 cells were derived from a primary tumour while MNT-1 originated from metastatic samples. Our previous study of mouse embryonic fibroblasts (MEFs) showed that TPC1 has an absolute level of mRNA expression that is much greater than that of TPC2 [39,40], and this might explain why we did not see significant changes in TPC2-deficient B16-F0 cells due to the relatively smaller expression of TPC2 compared to that of TPC1. In MNT-1 cells, however, TPC2 has been reported to be overexpressed [5], which as a result might have amplified the effect of TPC2 KO. As in the case of TPC2 KO CHL-1 cells, it would be worth checking the base level of MITF (i.e. its overexpression might still be at intermediate level), especially given the fact that CHL-1 cells have completely lost the ability to produce melanin. Also, previously we attributed the increased aggressiveness of CHL-1 TPC2 KO cells to the HIPPO pathway [14], which is completely independent from the mTORC1-TFEB-MITF axis. One should also note that TPC2, but not TPC1, is found on melanosomes and could directly affect melanogenesis, which would make the roles of TPC2 more complicated [41]. In summary, given the difference in distribution and level of expression, TPC1 and TPC2 might behave in distinct ways during the oncogenesis of melanoma, and we have for the first time revealed the significance of TPC1 in this process. Our findings therefore show that both TPC1 and TPC2 represent potential biomarkers and therapeutic targets for the diagnosis and treatment of melanoma, and also other types of cancer.

The major limitation of this study is that the roles of TPC1 in melanogenesis and tumourigenesis could be further validated in more types of cell or animal models, or using rescue assays to recover the phenotypes by expressing exogenous TPC1 or modulating mTORC1 with pharmacological inhibitors. Additionally, the hypothetic mTORC1-TFEB-MITF pathway would benefit from extra validation work, as the rheostat model of MITF *per se* is also controversial. The detailed mechanisms by which mTORC1 upregulates MITF and TFEB should also be further investigated and elucidated.

CRediT authorship contribution statement

Xuhui Jin: Writing – review & editing, Writing – original draft, Visualization, Validation, Software, Methodology, Investigation, Formal analysis, Data curation, Conceptualization. **Ali A. Hanbashi:** Resources, Methodology, Investigation, Conceptualization. **Faroq Kamli:** Investigation. **Xiaoqi Pan:** Investigation. **Colin R. Goding:** Writing – review & editing, Resources. **John Parrington:** Writing – review & editing, Resources, Project administration, Funding acquisition, Conceptualization.

Data availability

The data that support the findings of this study are available in the main text of this paper. Original images and detailed protocols are available on request from the corresponding author, J.P.

Funding

This work was supported by a grant from the CRUK Oxford Centre Development Fund.

Declaration of competing interest

The authors declare that they have no known competing financial interests or personal relationships that could have appeared to influence the work reported in this paper.

Appendix A. Supplementary data

Supplementary data to this article can be found online at https://doi.org/10.1016/j.heliyon.2024.e39752.

References

[1] S. Yi, S. Lin, Y. Li, W. Zhao, G.B. Mills, N. Sahni, Functional variomics and network perturbation: connecting genotype to phenotype in cancer, Nat. Rev. Genet. 18 (2017) 395–410.
[2] R. Nussinov, C.J. Tsai, H. Jang, Anticancer drug resistance: an update and perspective, Drug Resist. Updates 59 (2021) 100796.
[3] Y. Yuan, H. Li, W. Pu, L. Chen, D. Guo, H. Jiang, B. He, S. Qin, K. Wang, N. Li, J. Feng, J. Wen, S. Cheng, Y. Zhang, W. Yang, D. Ye, Z. Lu, C. Huang, J. Mei, H. F. Zhang, P. Gao, P. Jiang, S. Su, B. Sun, S.M. Zhao, Cancer metabolism and tumor microenvironment: fostering each other? Sci. China Life Sci. 65 (2022) 236–279.
[4] C.R. Goding, H. Arnheiter, MITF-the first 25 years, Genes Dev. 33 (2019) 983–1007.
[5] C. Abrahamian, C. Grimm, Endolysosomal cation channels and MITF in melanocytes and melanoma, Biomolecules 11 (2021).
[6] V. Bouché, A.P. Espinosa, L. Leone, M. Sardiello, A. Ballabio, J. Botas, Drosophila Mitf regulates the V-ATPase and the lysosomal-autophagic pathway, Autophagy 12 (2016) 484–498.
[7] A. Ballabio, J.S. Bonifacino, Lysosomes as dynamic regulators of cell and organismal homeostasis, Nat. Rev. Mol. Cell Biol. 21 (2020) 101–118.
[8] J. Ballesteros-Álvarez, R. Dilshat, V. Fock, K. Möller, L. Karl, L. Larue, M.H. Ögmundsdóttir, E. Steingrímsson, MITF and TFEB cross-regulation in melanoma cells, PLoS One 15 (2020) e0238546.
[9] A.J. Morgan, L.L. Martucci, L.C. Davis, A. Galione, Two-pore channels: going with the flows, Biochem. Soc. Trans. 50 (2022) 1143–1155.
[10] X. Jin, Y. Zhang, A. Alharbi, A. Hanbashi, A. Alhoshani, J. Parrington, Targeting two-pore channels: current progress and future challenges, Trends Pharmacol. Sci. 41 (2020) 582–594.
[11] M.X. Zhu, J. Ma, J. Parrington, P.J. Calcraft, A. Galione, A.M. Evans, Calcium signaling via two-pore channels: local or global, that is the question, Am. J. Physiol. Cell Physiol. 298 (2010) C430–C441.
[12] A.J. Morgan, F.M. Platt, E. Lloyd-Evans, A. Galione, Molecular mechanisms of endolysosomal Ca2+ signalling in health and disease, Biochem. J. 439 (2011) 349–374.
[13] S. Patel, B.S. Kilpatrick, Two-pore channels and disease, Biochim. Biophys. Acta Mol. Cell Res. 1865 (2018) 1678–1686.
[14] A. D'Amore, A.A. Hanbashi, S. Di Agostino, F. Palombi, A. Sacconi, A. Voruganti, M. Taggi, R. Canipari, G. Blandino, J. Parrington, A. Filippini, Loss of two-pore channel 2 (TPC2) expression increases the metastatic traits of melanoma cells by a mechanism involving the hippo signalling pathway and store-operated calcium entry, Cancers 12 (2020).
[15] P. Netcharoensirisuk, C. Abrahamian, R. Tang, C.C. Chen, A.S. Rosato, W. Beyers, Y.K. Chao, A. Filippini, S. Di Pietro, K. Bartel, M. Biel, A.M. Vollmar, K. Umehara, W. De-Eknamkul, C. Grimm, Flavonoids increase melanin production and reduce proliferation, migration and invasion of melanoma cells by blocking endolysosomal/melanosomal TPC2, Sci. Rep. 11 (2021) 8515.
[16] H. Swalwell, J. Latimer, R.M. Haywood, M.A. Birch-Machin, Investigating the role of melanin in UVA/UVB- and hydrogen peroxide-induced cellular and mitochondrial ROS production and mitochondrial DNA damage in human melanoma cells, Free Radic. Biol. Med. 52 (2012) 626–634.
[17] K.J. Livak, T.D. Schmittgen, Analysis of relative gene expression data using real-time quantitative PCR and the 2(-Delta Delta C(T)) method, Methods 25 (2001) 402–408.
[18] J. Schindelin, I. Arganda-Carreras, E. Frise, V. Kaynig, M. Longair, T. Pietzsch, S. Preibisch, C. Rueden, S. Saalfeld, B. Schmid, J.Y. Tinevez, D.J. White, V. Hartenstein, K. Eliceiri, P. Tomancak, A. Cardona, Fiji: an open-source platform for biological-image analysis, Nat. Methods 9 (2012) 676–682.
[19] T. Mosmann, Rapid colorimetric assay for cellular growth and survival: application to proliferation and cytotoxicity assays, J. Immunol. Methods 65 (1983) 55–63.
[20] M. Ruas, K.T. Chuang, L.C. Davis, A. Al-Douri, P.W. Tynan, R. Tunn, L. Teboul, A. Galione, J. Parrington, TPC1 has two variant isoforms, and their removal has different effects on endo-lysosomal functions compared to loss of TPC2, Mol. Cell Biol. 34 (2014) 3981–3992.
[21] S.A. D'Mello, G.J. Finlay, B.C. Baguley, M.E. Askarian-Amiri, Signaling pathways in melanogenesis, Int. J. Mol. Sci. 17 (2016).
[22] S. Shibahara, K. Takeda, K. Yasumoto, T. Udono, K. Watanabe, H. Saito, K. Takahashi, Microphthalmia-associated transcription factor (MITF): multiplicity in structure, function, and regulation, J. Investig. Dermatol. Symp. Proc. 6 (2001) 99–104.
[23] N. Fuse, K. Yasumoto, K. Takeda, S. Amae, M. Yoshizawa, T. Udono, K. Takahashi, M. Tamai, Y. Tomita, M. Tachibana, S. Shibahara, Molecular cloning of cDNA encoding a novel microphthalmia-associated transcription factor isoform with a distinct amino-terminus, J. Biochem. 126 (1999) 1043–1051.
[24] C.M. Takemoto, Y.J. Yoon, D.E. Fisher, The identification and functional characterization of a novel mast cell isoform of the microphthalmia-associated transcription factor, J. Biol. Chem. 277 (2002) 30244–30252.
[25] A. Oppezzo, F. Rosselli, The underestimated role of the microphthalmia-associated transcription factor (MiTF) in normal and pathological haematopoiesis, Cell Biosci. 11 (2021) 18.
[26] C.C. Dibble, L.C. Cantley, Regulation of mTORC1 by PI3K signaling, Trends Cell Biol. 25 (2015) 545–555.
[27] R. Zoncu, A. Efeyan, D.M. Sabatini, mTOR: from growth signal integration to cancer, diabetes and ageing, Nat. Rev. Mol. Cell Biol. 12 (2011) 21–35.
[28] C.R. Goding, Commentary. A picture of Mitf in melanoma immortality, Oncogene 30 (2011) 2304–2306.
[29] C. Settembre, C. Di Malta, V.A. Polito, M. Garcia Arencibia, F. Vetrini, S. Erdin, S.U. Erdin, T. Huynh, D. Medina, P. Colella, M. Sardiello, D.C. Rubinsztein, A. Ballabio, TFEB links autophagy to lysosomal biogenesis, Science 332 (2011) 1429–1433.
[30] E. Astanina, F. Bussolino, G. Doronzo, Multifaceted activities of transcription factor EB in cancer onset and progression, Mol. Oncol. 15 (2021) 327–346.
[31] S. Li, Y. Song, C. Quach, H. Guo, G.B. Jang, H. Maazi, S. Zhao, N.A. Sands, Q. Liu, G.K. In, D. Peng, W. Yuan, K. Machida, M. Yu, O. Akbari, A. Hagiya, Y. Yang, V. Punj, L. Tang, C. Liang, Transcriptional regulation of autophagy-lysosomal function in BRAF-driven melanoma progression and chemoresistance, Nat. Commun. 10 (2019) 1693.
[32] P.A. Ascierto, J.M. Kirkwood, J.J. Grob, E. Simeone, A.M. Grimaldi, M. Maio, G. Palmieri, A. Testori, F.M. Marincola, N. Mozzillo, The role of BRAF V600 mutation in melanoma, J. Transl. Med. 10 (2012) 85.
[33] K.G. de la Cruz López, M.E. Toledo Guzmán, E.O. Sánchez, A. García Carrancá, mTORC1 as a regulator of mitochondrial functions and a therapeutic target in cancer, Front. Oncol. 9 (2019) 1373.
[34] A. Jha, M. Ahuja, S. Patel, E. Brailoiu, S. Muallem, Convergent regulation of the lysosomal two-pore channel-2 by Mg^{2+}, NAADP, $PI(3,5)P_2$ and multiple protein kinases, EMBO J. 33 (2014) 501–511.
[35] O.A. Ogunbayo, J. Duan, J. Xiong, Q. Wang, X. Feng, J. Ma, M.X. Zhu, A.M. Evans, mTORC1 controls lysosomal Ca(2+) release through the two-pore channel TPC2, Sci. Signal. 11 (2018).
[36] C. Cang, Y. Zhou, B. Navarro, Y.J. Seo, K. Aranda, L. Shi, S. Battaglia-Hsu, I. Nissim, D.E. Clapham, D. Ren, mTOR regulates lysosomal ATP-sensitive two-pore Na(+) channels to adapt to metabolic state, Cell 152 (2013) 778–790.
[37] F.S. Chang, Y. Wang, P. Dmitriev, J. Gross, A. Galione, C. Pears, A two-pore channel protein required for regulating mTORC1 activity on starvation, BMC Biol. 18 (2020) 8.
[38] D. Ploper, E.M. De Robertis, The MITF family of transcription factors: role in endolysosomal biogenesis, Wnt signaling, and oncogenesis, Pharmacol. Res. 99 (2015) 36–43.
[39] M. Ruas, L.C. Davis, C.C. Chen, A.J. Morgan, K.T. Chuang, T.F. Walseth, C. Grimm, C. Garnham, T. Powell, N. Platt, F.M. Platt, M. Biel, C. Wahl-Schott, J. Parrington, A. Galione, Expression of Ca^{2+}-permeable two-pore channels rescues NAADP signalling in TPC-deficient cells, EMBO J. 34 (2015) 1743–1758.
[40] K.J. van Wijk, T. Leppert, Z. Sun, A. Kearly, M. Li, L. Mendoza, I. Guzchenko, E. Debley, G. Sauermann, P. Routray, S. Malhotra, A. Nelson, Q. Sun, E.W. Deutsch, Detection of the Arabidopsis proteome and its post-translational modifications and the nature of the unobserved (dark) proteome in PeptideAtlas, J. Proteome Res. 23 (2024) 185–214.
[41] N.W. Bellono, I.E. Escobar, E. Oancea, A melanosomal two-pore sodium channel regulates pigmentation, Sci. Rep. 6 (2016) 26570.